Roles of the Moisture and Wave Feedbacks in Shaping the Madden–Julian Oscillation

FEI LIU

Earth System Modeling Center, and Climate Dynamics Research Center, Nanjing University of Information Science and Technology, Nanjing, China

BIN WANG

Department of Atmospheric Sciences, and Atmosphere–Ocean Research Center, University of Hawai'i at Mānoa, Honolulu, Hawaii

(Manuscript received 2 January 2017, in final form 28 August 2017)

ABSTRACT

This study investigates the moisture and wave feedbacks in the Madden–Julian oscillation (MJO) dynamics by applying the general three-way interaction theoretical model. The three-way interaction model can reproduce observed large-scale characteristics of the MJO in terms of horizontal quadrupole-vortex structure, vertically tilted structure led by planetary boundary layer (PBL) convergence, slow eastward propagation with a period of 30–90 days, and planetary-scale circulation. The moisture feedback effects can be identified in this model by using diagnostic thermodynamic and momentum equations, and the wave feedback effects are investigated by using a diagnostic moisture equation. The moisture feedback is found to be responsible for producing the MJO dispersive modes when the convective adjustment process is slow. The moisture feedback mainly acts to reduce the frequency and growth rate of the short waves, while leaving the planetary waves less affected, so neglecting the moisture feedback is a good approximation for the wavenumber-1 MJO. The wave feedback is shown to slow down the eastward propagation and increase the growth rate of the planetary waves. The wave feedback becomes weak when the convective adjustment time increases, so neglecting the wave feedback is a good approximation for the MJO dynamics during a slow adjustment process. Sensitivities of these two feedbacks to other parameters are also discussed. These theoretical findings suggest that the two feedback processes, and thus the behaviors of the simulated MJO mode, should be sensitive to the parameters used in cumulus parameterizations.

1. Introduction

The Madden–Julian oscillation (MJO), as a significant driver of global circulation with a period of 30–90 days, is characterized by a zonal planetary scale and slow eastward propagation ($5\,m\,s^{-1}$) over the tropical Indian and western Pacific Oceans (Zhang 2005). The MJO has different spectral characteristics from the moist Kelvin waves, since its frequency is nearly independent of wavelength, whereas the frequency of the moist Kelvin waves increases with wavenumber linearly (Wheeler and Kiladis 1999).

To understand the observed features of the MJO, many theories have been presented in the past 30 years (Wang et al. 2016), including the following. 1) Frictional Kelvin–Rossby dynamics: This theory is rooted in the idea that the upward Ekman pumping in the planetary boundary layer (PBL) can couple the Kelvin and Rossby waves, and moisten the lower troposphere at the front of the convective center (Wang 1988; Wang and Rui 1990). 2) Moisture mode dynamics: In popular treatments of the moisture mode framework (Sobel and Maloney 2012, 2013; Adames and Kim 2016), the only prognostic variable is moisture, and circulation is assumed to have a balanced Gill response; in other words, circulation evolves in accordance to the evolution of precipitation. In another group of the moisture mode, circulation is also prognostic, and the cloud–radiation interaction and wind-induced surface heat exchange (WISHE) are the foci (Fuchs and Raymond 2005; Raymond and Fuchs 2007; Fuchs and Raymond 2017). 3) Multiscale interaction dynamics: The MJO is considered as a multiscale envelope. The high-frequency waves embedded in the MJO skeleton are assumed to be the instability

Corresponding author: Dr. Fei Liu, liuf@nuist.edu.cn

DOI: 10.1175/JCLI-D-17-0003.1

source for the MJO (Nakazawa 1988; Majda and Biello 2004; Majda et al. 2007; Majda and Stechmann 2009; Wang and Liu 2011; Liu et al. 2012; Liu and Wang 2012b, 2013b). 4) The gravity wave interference model: The MJO is thought as a large envelope of small-scale gravity waves triggered by individual convective cells (Yang and Ingersoll 2013, 2014).

In the convectively coupled Kelvin–Rossby wave theory, the change of moisture anomaly is neglected, and precipitation is parameterized by the assumption that it responds to the moisture convergence in both the lower troposphere and the PBL instantly (Wang and Rui 1990). In the idealized MJO model based on the moisture mode theory (Sobel and Maloney 2012, 2013), on the other hand, the momentum and geopotential height anomalies are diagnostic in accordance to precipitation evolution and the Gill response is used. Although the MJO shows a Gill pattern–like structure in the observation when its convective center is located over the Maritime Continent, its structure is different from the Gill pattern. The ratio of the maximum low-level westerly speed versus the maximum easterly speed in the Gill pattern is much larger than that for the MJO: the ratio is 2.2 for the Gill pattern, whereas it is only 1.3 for the observed MJO (Wang et al. 2016). This result means that the change of anomalous momentum and geopotential height may be important for the MJO dynamics. Thus, we define ''wave feedback'' as the change of anomalous momentum and geopotential height; that is, wave feedback is identified when the anomalous circulation is prognostic rather than diagnostic through a Gill response. Actually, the circulation always changes in association with the MJO convection whether it is prognostic or diagnostic. The wave feedback also exists when the circulation is diagnostic (Sobel and Maloney 2012, 2013; Adames and Kim 2016). Because of the important role of the change of anomalous circulation (Wang et al. 2016), we study this kind of wave feedback that represents the change of anomalous circulation in this work.

The ''moisture feedback'' is defined as the change of anomalous moisture, and the moisture feedback is identified when anomalous moisture is prognostic rather than neglected. The wave feedback and the moisture feedback are found to be important for explaining the MJO dynamics as individual feedbacks, although their relative roles were never discussed in these previous studies.

In the recently developed three-way interaction model, also known as the trio interaction model (Liu and Wang 2017; Wang and Chen 2017; Wang et al. 2016), both the moisture and wave feedbacks are included. Although it lacks the horizontal moisture advection process that can cause the eastward propagation of the MJO (Adames and Kim 2016; Liu and Wang 2016), a frictionally coupled dynamics moisture (FCDM) mode, coming from the interaction of diabatic heating, frictional wave dynamics and moisture dynamics, can also reproduce the planetary-scale characteristics of the MJO. In the three-way interaction model (Liu and Wang 2017; Wang and Chen 2017; Wang et al. 2016), the wave or circulation-induced PBL convergence is found to be an instability source for the MJO and to select the eastward propagation of the MJO. The moisture feedback, however, acts to delay the deep convection and slow down the eastward propagation of the coupled system. Since both the wave and moisture feedbacks are present simultaneously in the three-way interaction model, it remains unclear what roles these two types of feedbacks actually play in the MJO dynamics. Since most parameters were fixed in the previous studies, it remains unclear how sensitive these two feedbacks are to different parameter ranges.

In this paper, we will explore the relative roles of these two types of feedbacks in a single model, the general three-way interaction model. We will illustrate the parameter ranges over which the approximation of neglecting one of these two types of feedbacks is valid. To cause the eastward propagation of the MJO, there are some key processes such as the horizontal moisture advection by anomalous wind (Adames and Kim 2016; Liu and Wang 2016), the PBL moisture convergence (Liu and Wang 2012a), the WISHE (Fuchs and Raymond 2005), and the stratiform heating–induced zonal asymmetry (Wang et al. 2017). In this study, we only include the PBL effect.

Section 2 introduces the three-way interaction model and defines the wave and moisture feedbacks. The roles of moisture and wave feedbacks on the Kelvin wave are discussed in section 3. In section 4, the simulated FCDM mode with a coupled Rossby–Kelvin wave in the three-way interaction model is presented, and some sensitivity experiments are discussed. The relative roles of moisture and wave feedbacks on the MJO-like FCDM mode are discussed in sections 5 and 6, respectively. In section 7, we compare the theoretical results with observations. In section 8, we present a discussion and our conclusions.

2. The general three-way interaction model

a. Model framework

The theoretical model used here is the general three-way interaction model framework for the MJO (Liu and

Wang 2017; Wang and Chen 2017). This model extends the Matsuno–Gill (Matsuno 1966; Gill 1980) model by parameterizing precipitation through a simple Betts–Miller scheme (Betts 1986; Betts and Miller 1986; Frierson et al. 2004) and by including a combined interaction of diabatic heating, moisture dynamics, and frictional wave dynamics. This three-way interaction model, involving coupling of frictional wave dynamics and moisture mode dynamics, presents an MJO-like FCDM mode. This FCDM mode can capture significant planetary-scale characteristics of the MJO, including slow eastward propagation, planetary-scale selection, wavenumber-independent dispersion relationship, and vertically tilted structure caused by the PBL convergence (Liu and Wang 2017). By using the gravity wave velocity $C = 50\,\mathrm{m\,s^{-1}}$ as the reference speed, the temporal and spatial scale can be represented by $\sqrt{1/C\beta} = 8.5$ h and $\sqrt{C/\beta} = 1500$ km, respectively, where $\beta = 2.3 \times 10^{-11}\,\mathrm{m^{-1}\,s^{-1}}$ is the equatorial curvature effect of Earth to the first order. The nondimensional equations for the model are expressed as follows:

$$
\begin{aligned}
r_w u_t - yv &= -\phi_x - \varepsilon u,\\
r_w v_t + yu &= -\phi_y - \varepsilon v,\\
r_w \phi_t + (u_x + v_y) - w_b &= -p_r - \varepsilon\phi,\\
r_q q_t + \overline{Q}(u_x + v_y) - \overline{Q}_b w_b &= -p_r,\\
p_r &= \frac{1}{\tau}(q + \alpha\phi),\\
w_b &= d(d_1\phi_{xx} + d_2\phi_x + d_1\phi_{yy} + d_3\phi_y),
\end{aligned}
\tag{1}
$$

where u and v are the low-level horizontal wind anomalies in the zonal and meridional directions, respectively; ϕ is low-level geopotential anomaly; q is the column-integrated moisture anomaly; p_r is precipitation anomaly associated with convective heating; and w_b is vertical velocity anomaly caused by the PBL convergence. In addition, the subscripts t, x, and y denote the partial differentials of the variables in time t and space x and y, respectively. Also, $\varepsilon = 0.04$ is the nondimensional damping coefficient for momentum and temperature, set to 10 days in this study, and $\overline{Q} = 0.9$ and $\overline{Q}_b = 1.8$ are the nondimensional background moisture gradients (downward) in the low-level atmosphere and the PBL over a warm sea surface temperature (SST) of 29.5°C, respectively. The SST is the warmest in the tropics, which becomes colder poleward, and its e-folding damping scale is 30° (Kang et al. 2013). Thus, $\overline{Q}$ and $\overline{Q}_b$ also have an e-folding damping scale of 30°. The variable τ is the convective adjustment time originally used to measure how long the convection releases convective available potential energy (CAPE); τ is also used to represent the moisture relaxation time scale, and a convective adjustment time of 2.4 days has been used in the moisture mode theory (Sobel and Maloney 2012) and of a range of 0.5–1.0 days in the updated moisture mode theory with moisture advection (Adames and Kim 2016). Following the observation based on the precipitation-moisture curve (Adames and Kim 2016), a convective adjustment time of 13.7 h is used here, which has a nondimensional value of $\tau = 1.7$. Also, $\alpha = 0.1$ is a coefficient representing the role of environmental buoyancy on CAPE, and $d = 0.25$ is the nondimensional PBL depth of 100 hPa; and $d_1 = e/(e^2 + y^2)$, $d_2 = -(e^2 - y^2)/(e^2 + y^2)^2$, and $d_3 = -2ey/(e^2 + y^2)^2$, where $e = 1.1$ is the PBL friction of 8 h, and y is the nondimensional meridional distance away from the equator. More details of this three-way interaction model can be found in Wang and Chen (2017) and in Liu and Wang (2017).

The variables r_w and r_q are the tracers with a value of 1 or 0 to switch on and off the wave feedback and moisture feedback, respectively. A value of $r_w = 0$ reduces the model to a model for the frictionally coupled moisture (FCM) mode, in which the wave feedback is turned off and the circulation will respond to moisture process instantly, as it does in the moisture mode theory. A value of $r_q = 0$ changes the three-way interaction model to a model for the frictionally coupled dynamic (FCD) mode, in which the moisture feedback is turned off and precipitation responds to moisture convergence instantly, as it does in the frictional wave dynamics. Otherwise, these two coefficients are set to 1, resulting in the full model for the FCDM mode.

The convective adjustment time τ, the wave damping coefficient ε, and the PBL depth d are three important parameters. Sensitivity experiments on these parameters are discussed in the following sections.

b. Eigenvalue problem

Following Liu and Wang (2017), this linear three-way interaction model of Eq. (1) can be calculated through solving the eigenvalue problem. For the zonally propagating equatorial waves, their structure can be specified to have a form of $\exp[i(kx - \sigma t)]$, where σ is frequency, and k is wavenumber. The phase speed and growth rate of these equatorial waves can be represented by $\mathrm{Re}(\sigma)/k$ and $\mathrm{Im}(\sigma)$, respectively. The energy propagation speed is represented by $\mathrm{Re}(\partial\sigma/\partial k)$. After projecting the linear model onto the frequency–wavenumber space, a linear matrix for these five predicted variables in Eq. (1) is obtained, and the eigenvalue and eigenvector can be solved by the matrix inversion method. The meridional structure is expanded by using the parabolic cylinder functions. In this calculation, only the first three meridional modes of the parabolic cylinder functions are

used to represent the lowest meridional modes of the equatorial Rossby and Kelvin waves.

3. Different simple modes for Kelvin wave

a. The FCDM-mode Kelvin wave

Before calculating the three-way interaction model, let us consider an even simpler case of flow above the equator (i.e., the Kelvin wave). In this case, v is set to zero. For simplicity, the role of environmental buoyancy on CAPE is neglected ($\alpha = 0$). Sensitivity experiments show that neglecting this term does not change the results qualitatively. The formula for this three-way interaction model on the equator can be written as follows:

$$\begin{aligned} r_w u_t &= -\phi_x - \varepsilon u, \\ r_w \phi_t + u_x - w_b &= -p_r - \varepsilon \phi, \\ r_q q_t + \overline{Q} u_x - \overline{Q}_b w_b &= -p_r, \\ p_r &= \frac{1}{\tau} q, \\ w_b &= dd_1 \phi_{xx} + dd_2 \phi_x - dd_1 u, \end{aligned} \tag{2}$$

whose dispersion equation can be derived as

$$\begin{aligned} &r_q r_w^2 \tau \sigma^3 + [r_q(idd_1\tau k^2 + dd_2 \tau k + 2i\varepsilon\tau) + ir_w] r_w \sigma^2 \\ &+ [r_w dd_1(\overline{Q}_b - 1)k^2 - r_q \tau(\varepsilon dd_1 + 1)k^2 + ir_q d(\varepsilon d_2 + d_1)\tau k - ir_w dd_2(\overline{Q}_b - 1)k - r_q \varepsilon^2 \tau - 2r_w \varepsilon]\sigma \\ &+ \varepsilon dd_1(\overline{Q}_b - 1)ik^2 + (\overline{Q} - 1)ik^2 + (\varepsilon d_2 + d_1)(\overline{Q}_b - 1)dk - i\varepsilon^2 = 0. \end{aligned} \tag{3}$$

Details on how this dispersion equation is obtained can be found in the appendix.

For each positive wavenumber k, the damped westward-propagating solutions with negative real and imaginary parts of the frequency are not discussed. Figure 1a shows the simulated dispersion relationship of Kelvin waves for the FCDM, FCD, and FCM modes. The frequency of the FCDM mode, corresponding to the period of 10–30 days, weakly depends on wavelength, and the short waves have lower frequencies than the long waves. The FCD mode has a moist Kelvin wave–like dispersion relationship, demonstrated by frequency increasing with wavenumber. The FCM mode has higher frequency for the long waves than for the short waves, and its frequency of the planetary waves is also higher than that of the FCDM mode. Thus, the moisture feedback, represented by the difference between the FCDM and FCD modes, acts to slow down the eastward propagation of the short waves. The wave feedback represented by the difference between the FCDM and FCM modes, however, acts to slow down the planetary waves.

Figure 1b show the growth rates of these three modes. The FCDM and the FCM modes have a scale selection feature, and their planetary waves have stronger growth rate than the short waves. For the long waves, the FCM mode has a little larger growth rate than the FCDM mode, which means that the wave feedback tends to suppress planetary waves. The growth rate of the FCD mode, however, increases quickly with wavenumber. This difference between the FCDM and FCD modes means that the moisture feedback will damp the short waves quickly.

b. The FCD-mode Kelvin wave

The moisture feedback can be removed by setting $r_q = 0$. If we plug the Betts–Miller scheme into the moisture equation of Eq. (1), this moisture tendency term can also be removed in the special case of setting $\tau = 0$. This means the removal of the moisture feedback is a special case in which there is no buildup of CAPE, and the waves will "discharge" CAPE instantaneously. At this limit, the Kuo-type parameterization scheme is obtained (Wang and Chen 2017), in which precipitation is parameterized by both the tropospheric and PBL moisture convergence. When neglecting the tropospheric damping and the moisture feedback and using the longwave approximation in the PBL, Eq. (3) can be reduced to

$$\sigma^2 = i\overline{Q}_b dd_1 k + (1 - \overline{Q})k^2, \tag{4}$$

which is identical to the frictional moist Kelvin wave. Since $\overline{Q}_b dd_1 k$ is positive, the real part and imaginary part of the frequency should have the same sign. For the unstable solution with positive growth rate, the phase speed should be eastward, and the growth rate increases with wavenumber. Since $(1 - \overline{Q})$ is always positive for the intraseasonal time scale (Wang 1988), the instability is caused by the PBL moisture convergence.

c. The FCM-mode Kelvin wave

The wave feedback can be removed by setting $r_w = 0$. Since $\varepsilon = 0.04$ is very small for a standard tropospheric damping of 10 days, ε^2 is negligible compared to k^2. Thus, Eq. (3) becomes

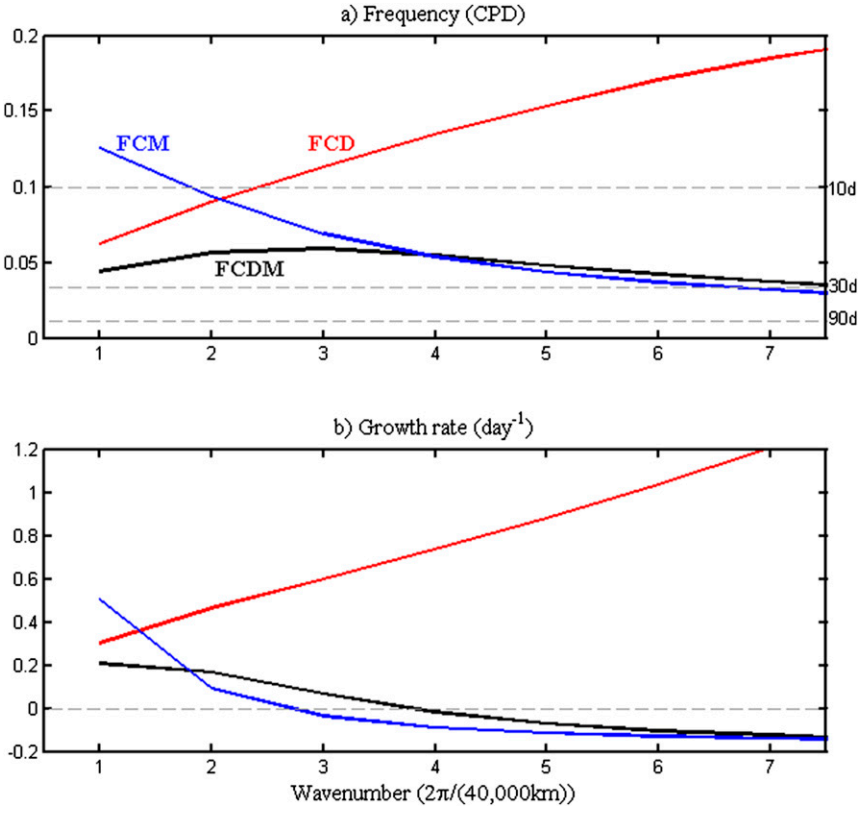

FIG. 1. Different simple modes for the Kelvin waves. Shown are (a) the frequency (cycles per day) and (b) growth rate (day^{-1}) as a function of wavenumber for the flow on the equator for the FCDM mode ($r_w = 1$ and $r_q = 1$; black), FCM mode ($r_w = 0$ and $r_q = 1$; blue), and FCD mode ($r_w = 1$ and $r_q = 0$; red).

$$\sigma = -i\tau^{-1}\left(1 - \frac{b_1\overline{Q}}{b_1^2 + b_2^2k^{-2}}\right) + i\tau^{-1}\overline{Q}_b\left(1 - \frac{b_1}{b_1^2 + b_2^2k^{-2}}\right) + \tau^{-1}(\overline{Q}_b - \overline{Q})\frac{b_2k}{b_1^2k^2 + b_2^2}, \tag{5}$$

where $b_1 = \varepsilon dd_1 + 1$ and $b_2 = \varepsilon dd_2 + dd_1$. The phase speed is $\tau^{-1}(\overline{Q}_b - \overline{Q})b_2/(b_1^2k^2 + b_2^2)$, and the eastward propagation is mainly induced by the inclusion of PBL dynamics. This means that PBL convergence can induce the eastward propagation of the MJO, being consistent with previous theoretical works (Liu and Wang 2012a, 2017).

The growth rate coming from the PBL dynamics, that is, $i\tau^{-1}\overline{Q}_b[1 - b_1/(b_1^2 + b_2^2k^{-2})]$, decreases with increasing wavenumber, which means that the PBL dynamics prefers the planetary scale in terms of instability. The reason is that, in this nondimensional equation, the circulation causing the PBL convergence is relatively weaker compared to the precipitation for the short waves than for the long waves. This relationship can be represented by the ratio of geopotential height to precipitation amplitude, that is, $\varepsilon^2/(b_1^2k^4 + b_2^2k^2)$, which decreases with increasing wavenumber. In this three-way interaction model, the diabatic heating associated with precipitation of short waves is mostly balanced by wind divergence.

4. Dynamics of FCDM mode in the three-way interaction model

Because of the important coupling of Rossby and Kelvin waves in the MJO, in this and following sections we further study the full three-way interaction model, which couples both Rossby and Kelvin waves. The eigenvalue and eigenvectors of Eq. (1) are then calculated.

a. Solution of the linear FCDM mode

Figure 2 shows the simulated dispersion relationship and instability of the FCDM mode in this three-way interaction model. The simulated frequency, corresponding to the period of 30–90 days, weakly depends on wavelength. The wavenumber 1 has an eastward propagation speed of 6.2 $m\,s^{-1}$, and wavenumber 2 has

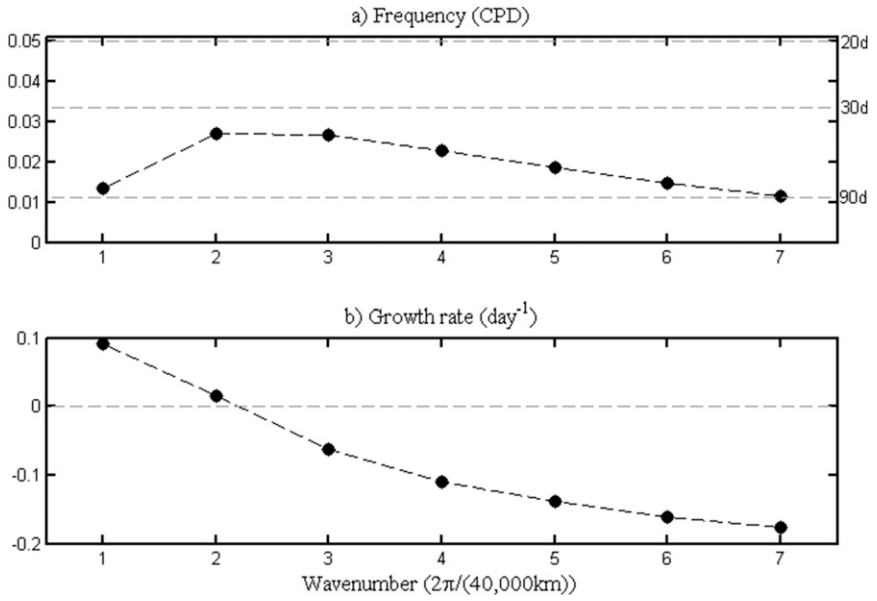

FIG. 2. Simulated FCDM mode: (a) frequency (cycles per day) and (b) growth rate (day^{-1}) as a function of wavenumber for the FCDM mode.

an eastward propagation speed of $6.3\,m\,s^{-1}$. This simulated dispersion relationship agrees with the observed one of the MJO very well, whose frequency is nearly independent of wavelength (Wheeler and Kiladis 1999; Kiladis et al. 2009). This dispersion relationship is different from that of the moist Kelvin waves, which has high frequency for the short waves. Compared to the simulated Kelvin waves with a period of 10–30 days in the three-way interaction model (Fig. 1a), the FCDM mode has a lower frequency. These results suggest that compared to the Kelvin waves, the coupling of Rossby waves will slow down the eastward propagation. Different from the moisture mode with a convective adjustment time in the range of 0.5–1.0 days, which simulates the westward energy propagation for the planetary waves (Adames and Kim 2016), the energy of the planetary waves for the FCDM mode has an eastward propagation speed of $6.4\,m\,s^{-1}$, whereas that of the short waves has a westward propagation speed of $-1.7\,m\,s^{-1}$. The simulated FCDM mode also has a scale selection feature in terms of instability, and the planetary waves have stronger growth rate than the short waves (Fig. 2b). These results indicate that the effect of the moisture feedback coupled to the PBL dynamics plays a critical role in selecting planetary waves for eastward propagation and growth.

Figure 3 shows the horizontal structure of the simulated FCDM mode. For this unstable eastward propagating wavenumber 1, a Gill-like structure is simulated. The upward Ekman pumping, which is nearly in phase with the anomalous geopotential height under the anomalous easterly wind, leads the convective center to the east by a phase of 0.2π, which is in agreement with the observations (Hendon and Liebmann 1994; Maloney and Hartmann 1998; Sperber 2003; Tian et al. 2006; Hsu and Li 2012). Also consistent with the observations (Chen and Wang 2017), the simulated equatorial geopotential anomaly is nearly out of phase with precipitation, and the precipitation center lags the minimum geopotential anomaly by 0.2π, which means a strong generation of eddy available potential energy (EAPE) for the wavenumber-1 FCDM mode. The unstable wavenumber-2 mode has a stronger Rossby component than the wavenumber-1 mode, and it shows a quadrupole-vortex structure (Fig. 3b). The negative equatorial geopotential anomaly center leads the convective center by a phase of 0.3π, which is larger than that of wavenumber 1. This means the wavenumber-2 mode should have smaller EAPE than the wavenumber-1 mode.

Figure 4 shows the EAPE generation for different wavelengths of the FCDM mode. The simulated EAPE is much larger for the long waves than for the short waves. Since the Betts–Miller parameterization introduces a strong damping effect in the moisture equation, the weak positive EAPE cannot make the short waves grow (Fig. 2b).

This new FCDM mode is similar to the moisture mode presented by Fuchs and Raymond (Fuchs and Raymond 2005; Fuchs and Raymond 2017). The FCDM mode is destabilized by PBL moisture convergence, while the moisture mode is by the cloud–radiation interaction and the WISHE.

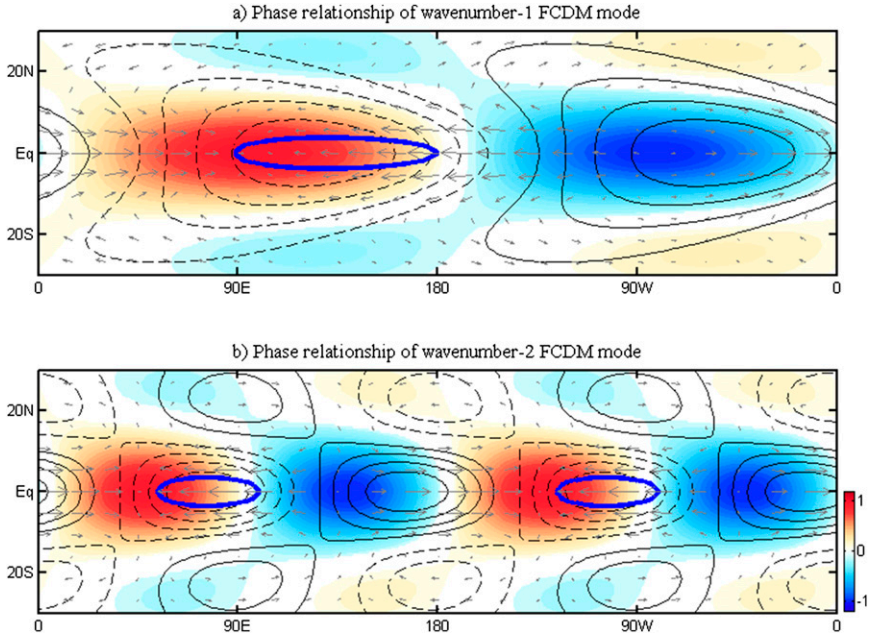

FIG. 3. Horizontal structures of the FCDM mode. Shown are horizontal structures of normalized precipitation anomalies (shading), lower-tropospheric geopotential height anomalies (black contours), lower-tropospheric velocity (vectors), and Ekman pumping (blue contours) for eastward-propagating (a) wavenumber-1 and (b) wavenumber-2 FCDM modes. The solid (dashed) contours denote positive (negative) anomalies. The contour interval is 0.2, and the zero contour is not shown. The thick blue contour denotes upward Ekman pumping with an amplitude of 0.7.

b. *Sensitivities of the FCDM mode to model parameters*

The solution of this linear FCDM mode is parameter dependent. Figure 5 shows the responses of frequency and growth rate to different convective adjustment times, wave damping times, and PBL depths. For a fast convective adjustment process of 6 h, the short waves have higher frequencies than the long waves (Fig. 5a). This is similar to the frictional moist Kelvin waves (Liu and Wang 2017). When the convective adjustment process slows down to 13.7 h, the frequency is reduced to the realistic MJO ranges for all wavenumbers, and the short waves are reduced significantly. For a very slow convective adjustment process of 48 h, frequency of the short waves is further reduced, and the westward energy propagation can also be simulated for the planetary waves, which has a speed of $-0.3\,\mathrm{m\,s^{-1}}$. The growth rate of the planetary waves is increased when the convective adjustment time decreases, whereas the short waves have the opposite results.

The tropospheric damping mainly affects the planetary waves (Fig. 5b), and a strong damping will reduce the frequency of all wavenumbers and weaken the instability of the long waves. The PBL effect also changes the FCDM mode significantly (Fig. 5c). When the PBL effect becomes strong with a large PBL depth, the frequency of wavenumber 1 is reduced, whereas that of the short waves is increased. The growth rate for all wavenumbers is increased when the PBL effect becomes

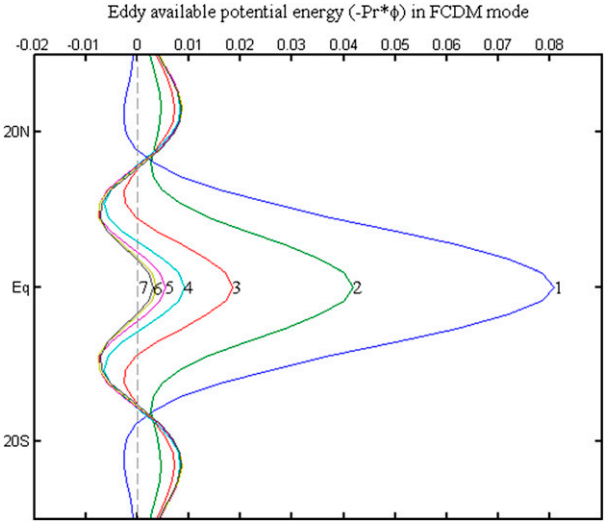

FIG. 4. Simulated EAPE for different wavenumbers of the FCDM mode. Shown are EAPE $-p_r\phi$ for wavenumbers 1–7 of the FCDM mode.

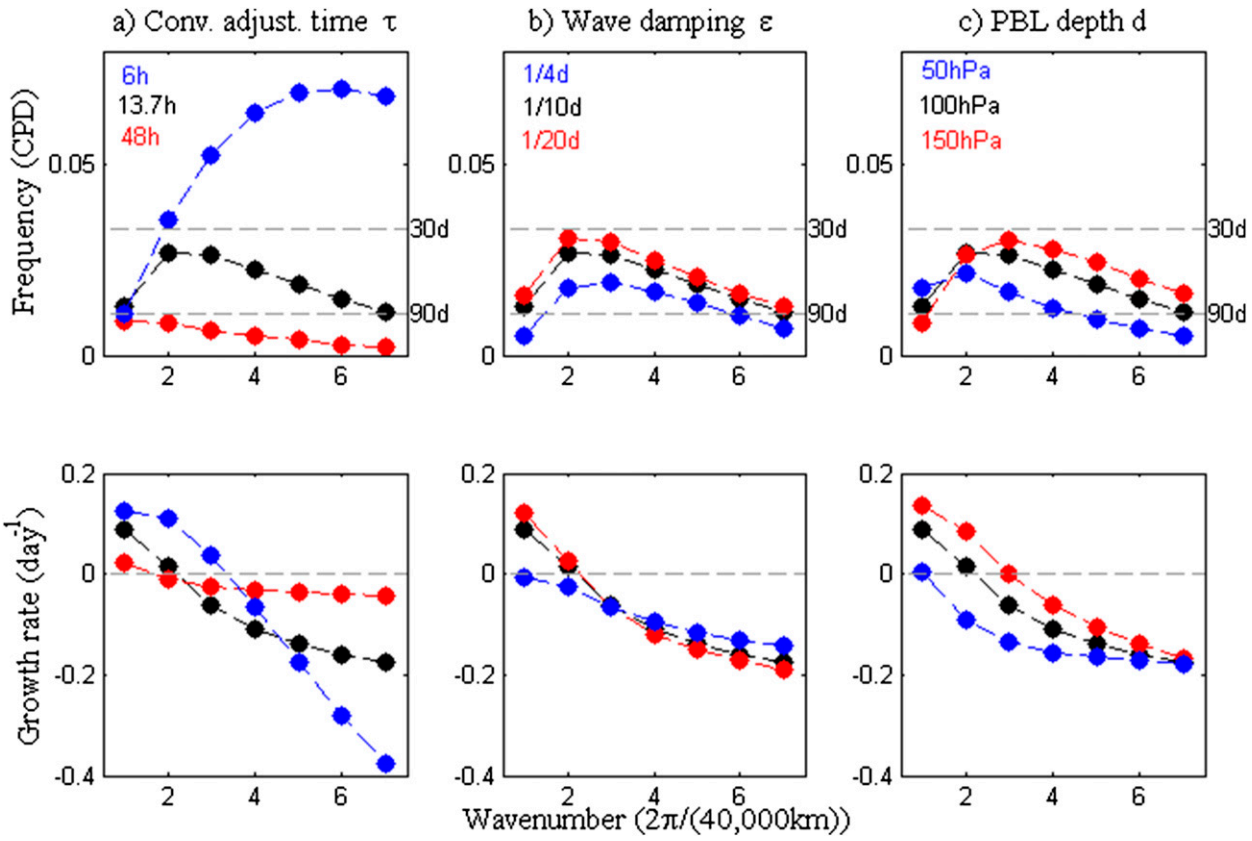

FIG. 5. Sensitivity experiments for the FCDM mode. (top) Simulated frequency (cycles per day) and (bottom) growth rate (day^{-1}) as a function of wavenumber with respect to different (a) convective adjustment times, (b) wave damping, and (c) PBL depths in the FCDM mode.

strong, which means that the PBL effect acts as an instability source for the unstable waves.

The model sensitivities to other parameters, such as the vertical background moisture gradient $\overline{Q}$ and the PBL friction e, are also examined. The sensitivity experiments show that results similar to those in Fig. 2 can be obtained in a broad range for these two parameters, while a strong vertical background moisture gradient will decrease the frequency and increase the growth rate for all wavenumbers. They also show that strong PBL friction tends to decrease both frequency and growth rate for all wavenumbers (figure not shown).

5. Roles of the moisture feedback

The roles of the moisture feedback can be represented by the difference between the FCDM and FCD modes. Figure 6 compares the simulated frequency and growth rate for the FCDM and FCD modes. The FCD mode only has a moist Kelvin wave–like dispersion relationship, for which the frequency increases with wavenumber. In general, the FCD mode has higher frequency and a more unstable mode than the FCDM mode, and the difference between the FCDM and FCD modes is most significant for the short waves. The simulated moisture feedback tends to reduce the frequency and growth rate of the short waves, while leaving the planetary waves less affected. Compared to the FCD mode that has increasing frequency with large wavenumber, the frequency is almost the same for all wavenumbers in the FCDM mode with moisture feedback. This moisture feedback is similar to that obtained from the pure Kelvin waves without coupling with the Rossby waves (Fig. 1).

Figure 7 exhibits the horizontal structure of the FCD mode. A structure similar to that in the FCDM mode is simulated for both wavenumbers 1 and 2, and the upward Ekman pumping, in phase with negative geopotential anomaly, leads the convective center to the east. The simulated Rossby component, however, is weaker than that in the FCDM mode. Compared to the FCDM mode (Fig. 3b), a Gill-like pattern rather than the quadrupole-vortex structure is simulated for the

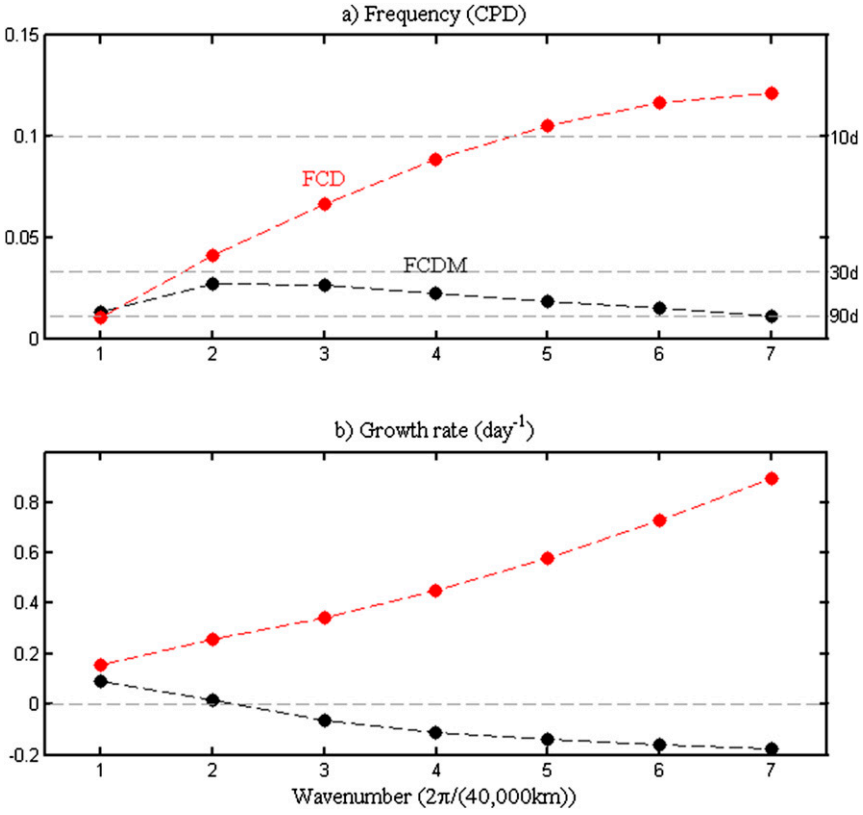

FIG. 6. As in Fig. 2, but for the simulated FCD mode (red). The frequency and growth rate in the FCDM mode (black) are also shown for comparison.

wavenumber-2 FCD mode (Fig. 7b), which means that the moisture feedback will enhance the Rossby component in the coupled Kelvin–Rossby system.

The phase lag between the upward Ekman pumping and convective center of the wavenumber-2 FCD mode is only 0.2π, which is much smaller than 0.3π for the wavenumber-2 FCDM mode. This means that the inclusion of the moisture feedback simulates a larger phase lag between the PBL convergence and precipitation compared to the pure wave dynamics. From the moisture equation, the inclusion of the moisture feedback means that the upward PBL Ekman pumping acts to precondition the lower troposphere or to enhance precipitation rather than to form precipitation directly; this indicates that the moisture feedback will delay the occurrence of precipitation and slow down the eastward propagation.

The delayed precipitation caused by the moisture feedback can be clearly seen in Fig. 8, which shows the time difference between the centers of PBL upward Ekman pumping, and precipitation in the FCDM and FCD modes, respectively. In the FCD mode, the precipitation center lags the upward Ekman pumping by less than 3 days for all wavenumbers except wavenumber 1. In the FCDM mode, however, it takes a long time, more than 5 days, for precipitation to occur after the upward Ekman pumping in the PBL.

With the standard parameters, the moisture feedback tends to reduce the frequency and growth rate of the short waves. Figure 9 shows the sensitivities of the moisture feedback to different parameters. This kind of moisture feedback is stable for different convective adjustment times, tropospheric damping times, and PBL depths, except that its effect on reducing the frequency of the short waves becomes weak for a very quick convective adjustment process of 6 h (Fig. 9a) or for a large PBL depth (Fig. 9c). In a broad range of parameters, the moisture feedback mainly affects the short waves while wavenumber 1 is less affected, which means neglecting the moisture feedback is a good approximation for the wavenumber-1 MJO.

6. Roles of the wave feedback

In common treatments of the moisture mode framework (Sobel and Maloney 2012, 2013; Adames and Kim 2016), moisture is the only prognostic variable, and the other fields evolve according to the evolution of precipitation, which is coupled to moisture. Thus, the FCM

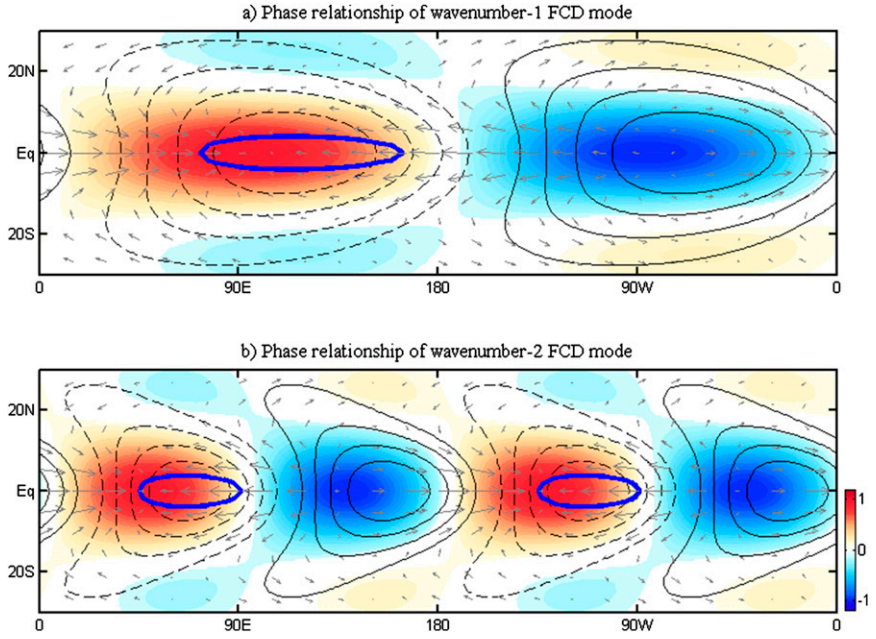

FIG. 7. As in Fig. 3, but for the horizontal structures of the FCD mode.

model, in which the circulation response is specified in accordance to the evolution of precipitation, can be seen as a variant of the moisture mode where the PBL dynamics is included, which induces eastward phase propagation. The other processes that can also cause eastward propagation (Fuchs and Raymond 2005; Adames and Kim 2016; Liu and Wang 2016; Wang et al. 2017), however, are not considered.

The role of the wave feedback can be represented by the difference between the FCDM and FCM modes. Figure 10 shows the frequency and growth rate for these two modes. The FCM mode has similar short waves as the FCDM mode, whereas for the planetary waves the simulated FCM mode presents much higher frequency and lower growth rate than the simulated FCDM mode does. This implies that the wave feedback has a large role in slowing down the eastward propagation and increasing the growth rate of the planetary waves. For the pure Kelvin waves without coupling with the Rossby waves, although the wave feedback can slow down the eastward propagation (Fig. 1a), it tends to decrease the growth rate of the planetary waves (Fig. 1b). This difference between the pure Kelvin wave and the coupled Kelvin–Rossby wave systems means that the coupling of Rossby and Kelvin waves is important for understanding the wave feedback.

Figure 11 exhibits the horizontal structure of the FCM mode, which has a similar structure to that of the FCDM mode (Fig. 3). The Rossby component of the FCM mode, however, is much stronger than that of the FCDM mode; thus, the equatorial geopotential anomalies of the former are much weaker than those of the latter. Since the precipitation anomaly is a maximum at the equator, which is caused by the equatorially trapped background SST and associated background moisture, the weakening of the equatorial Kelvin waves of the FCM mode should decrease this instability. As shown in Fig. 12, the EAPE of the FCM

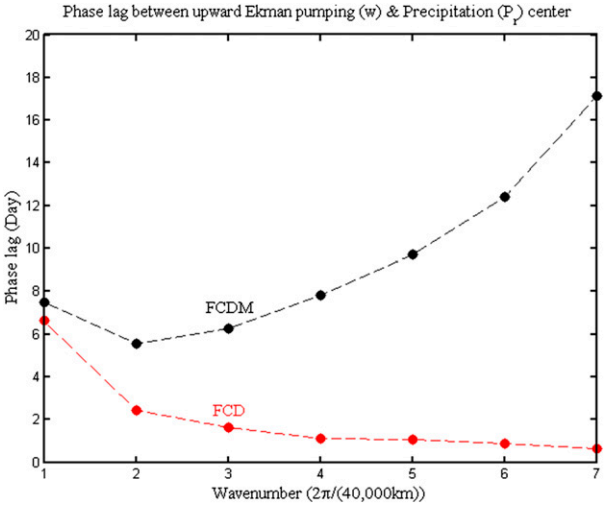

FIG. 8. Delay of precipitation occurrence by the moisture feedback. Time difference between upward Ekman pumping and precipitation center as a function of wavenumber in the FCDM mode (black) and in the FCD mode (red).

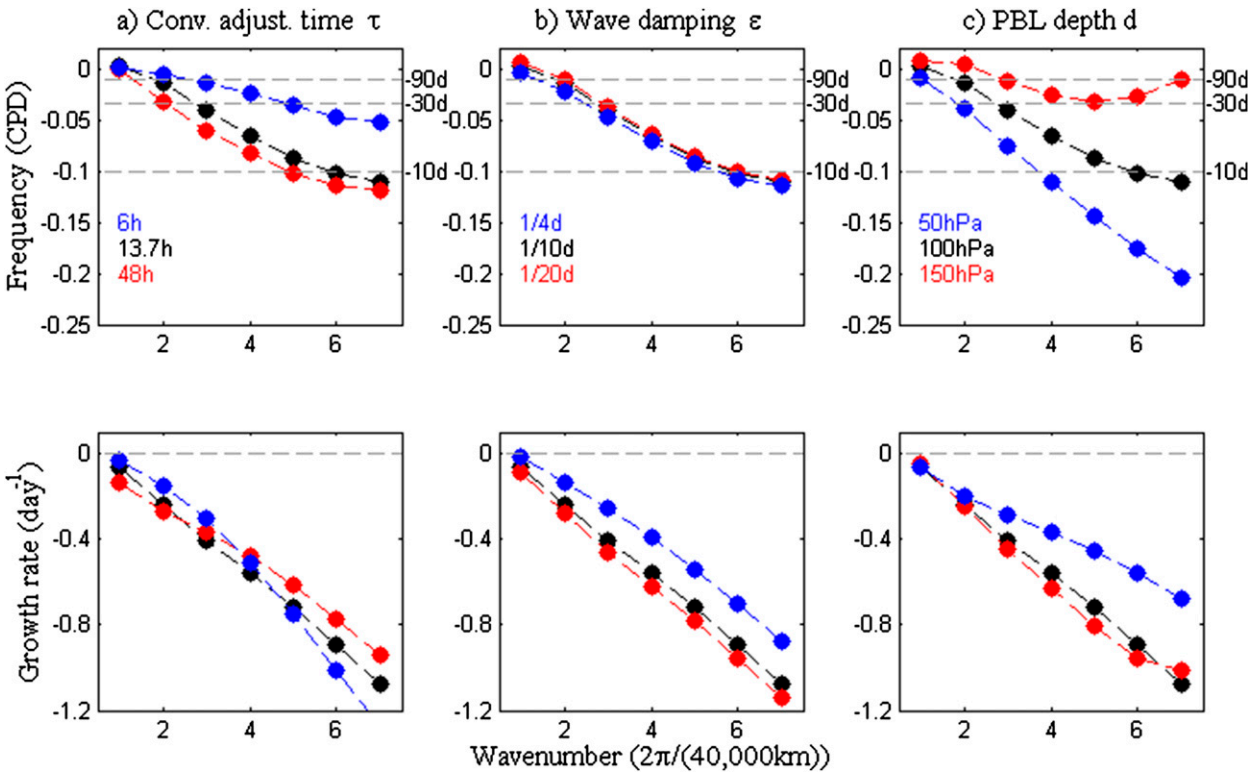

FIG. 9. Sensitivity experiments for the moisture feedback. Difference of (top) simulated frequency (cycles per day) and (bottom) growth rate (day^{-1}) between the FCDM and FCD modes as a function of wavenumber with respect to different (a) convective adjustment times, (b) wave damping, and (c) PBL depths.

mode is much smaller than that of the FCDM mode (Fig. 4). In summary, the wave feedback will weaken the Rossby component while enhancing the Kelvin component of this coupled system; thus, it will enhance the growth rate of the planetary waves.

The wave feedback is found to slow down the eastward propagation and increase the growth rate of the planetary waves (Fig. 10). Figure 13 shows how sensitive the wave feedback is to different convective adjustment times, wave damping times, and PBL depths. The role of the wave feedback becomes weak when the convective adjustment process becomes slow (Fig. 13a). This result means that neglecting the wave feedback is reasonable if a slow convective adjustment process is assumed. If we substitute the Betts–Miller scheme into the thermodynamics equation, we have the relationship $\phi_t \sim q/\tau$, which implies that the wave feedback has the same time scale as the CAPE discharge does in the Betts–Miller scheme. In the recent observational study (Adames 2017), the convective adjustment time was found to vary in space and time; thus, there are times when the wave feedback matters.

Associated with a weaker tropospheric damping (Fig. 13b), the role of the wave feedback in slowing down the eastward propagation becomes more dominant, and its effect of increasing the instability becomes stronger. A larger PBL depth will enhance the effect of the wave feedback in slowing down the eastward propagation, while weakening its role in increasing the instability of wavenumber-1 MJO (Fig. 13c).

7. Comparison with observations

The moisture feedback and wave feedback, two important processes for understanding the MJO dynamics, are studied in a theoretical three-way interaction model for the MJO with the presence of the PBL dynamics. For reference, the observational wavenumber–frequency power spectrum, eastward propagation, and horizontal structure of the MJO are shown in Fig. 14. The daily mean Advanced Very High Resolution Radiometer (AVHRR) interpolated outgoing longwave radiation (OLR) data from the National Oceanic and Atmospheric Administration (NOAA) satellites (Liebmann and Smith 1996) are used as an indicator of convection activity, and the daily mean winds from National Centers for Environmental Prediction (NCEP)–National Center for Atmospheric Research (NCAR) reanalysis project (Kalnay et al. 1996) are used to study the MJO circulation.

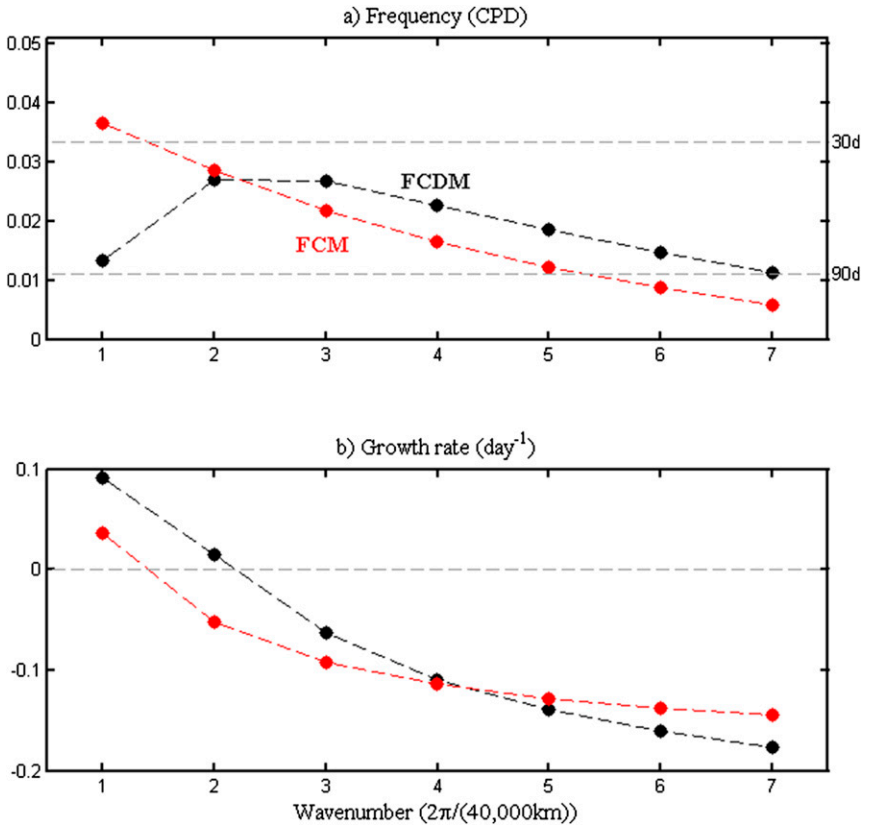

FIG. 10. As in Fig. 2, but for the simulated FCM mode (red). The frequency and growth rate in the FCDM mode (black) are also shown for comparison.

The results show that for the adjustment time of 13.7 h, an "MJO like" dispersion relationship can be simulated for the FCDM mode when both the moisture and wave feedbacks are included. The oscillation has a period of 30–90 days for the unstable wavenumbers 1 and 2, and the frequency is nearly independent of wavelength (Fig. 2). This dispersion relationship, different from that of the moist Kelvin wave, agrees with that of the observed MJO (Wheeler and Kiladis 1999; Zhang 2005; Kiladis et al. 2009), as shown in Fig. 14a. The simulated wavenumber 1, having an eastward propagation speed of 6.2 m s^{-1}, is consistent with the observed MJO over the Indo–western Pacific region (Fig. 14b).

In the observations, the convective center of the MJO is preceded by the PBL moisture convergence (Hendon and Liebmann 1994; Maloney and Hartmann 1998; Sperber 2003; Tian et al. 2006; Hsu and Li 2012), as shown by the 850-hPa upward motion to the east of the convective center in Fig. 14c. This vertical structure is also simulated for the FCDM mode in the three-way interaction model (Fig. 3). The instability, caused by additional moisture via the Ekman pumping to the east of the precipitation, is the strongest for the planetary waves (Fig. 4). Such PBL dynamics do provide one mechanism for understating why the MJO prefers the planetary scale.

For the MJO dynamics, the coupling of Rossby and Kelvin waves plays an important role. The MJO usually shows a Gill-like structure in the lower troposphere (Fig. 14c) and a quadrupole-vortex structure in the upper troposphere (Fig. 14d). The quadrupole-vortex feature of MJO has been documented in many previous studies (Rui and Wang 1990; Hendon and Salby 1994; Kiladis et al. 2005), which is mainly contributed by the Rossby waves (Wang and Rui 1990; Majda and Stechmann 2009). The simulated wavenumber-1 FCDM mode exhibits a Gill-like structure (Fig. 3a), and the quadrupole-vortex structure is also simulated for the wavenumber-2 FCDM mode (Fig. 3b). Without coupling with the Rossby waves, the wavelength-independent frequency relationship can also be simulated for the Kelvin waves when the PBL dynamics are present, while the simulated frequency with a period of 10–30 days is much higher than that when the Rossby waves are coupled.

With a slow convective adjustment process, the westward energy propagation and eastward phase

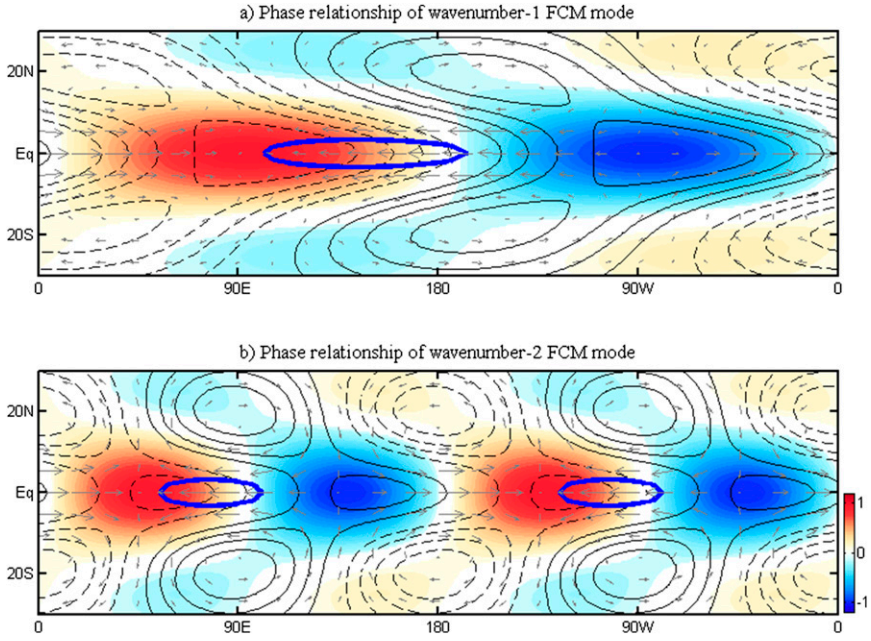

FIG. 11. As in Fig. 3, but for the horizontal structures of the FCM mode.

propagation can be simulated for the planetary waves in the FCDM model (Fig. 5a), which agrees well with the observation (Adames and Kim 2016). For a somewhat quick convective time scale in the range of 0.5–1.0 days, the westward energy propagation can be simulated for the planetary waves for the moisture mode (Adames and Kim 2016), whereas it only occurs for the short waves and the planetary waves show eastward energy propagation for the FCDM mode.

8. Discussion

Based on good MJO simulations in this three-way interaction model or the FCDM model, we can study the moisture and wave feedbacks explicitly. The moisture feedback mainly works to reduce the frequency and growth rate of the short waves and produce a dispersion relationship in which the frequency is almost the same for all wavenumbers (Figs. 6 and 9), which means that the moisture feedback is critical for simulating the MJO-like wavelength-independent dispersion relationship. The moisture feedback is very weak in changing planetary waves, thus neglecting the moisture feedback is a good approximation for simulating the wavenumber-1 MJO. The wave feedback mainly works to slow down the eastward propagation and increase the growth rate of the planetary waves (Fig. 10). Since the wave feedback is found to be weak when the convective adjustment process becomes slow (Fig. 13a), neglecting the wave feedback is a good approximation for the MJO when focusing on a slow convective adjustment process. In this coupled Kelvin–Rossby system, the moisture feedback tends to enhance the Rossby component (Figs. 3 and 7), while the wave feedback will weaken the Rossby component (Figs. 3 and 11).

The new findings in this work should improve our understanding of the MJO dynamics. Some other processes, such as the longwave radiation feedback (Chikira 2014; Kim et al. 2015), the multiscale interaction (Wang and Liu 2011; Liu and Wang 2012b, 2013b), and the air–sea interaction (Wang and Xie 1998; Liu and Wang 2013a), are

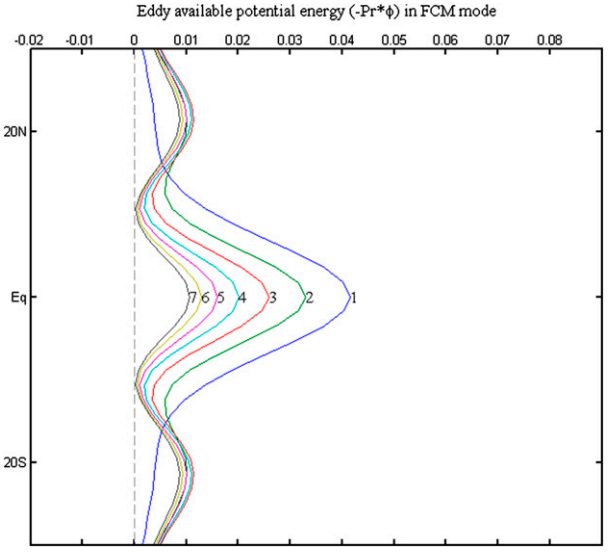

FIG. 12. As in Fig. 4, but for the simulated EAPE for different wavenumbers of the FCM mode.

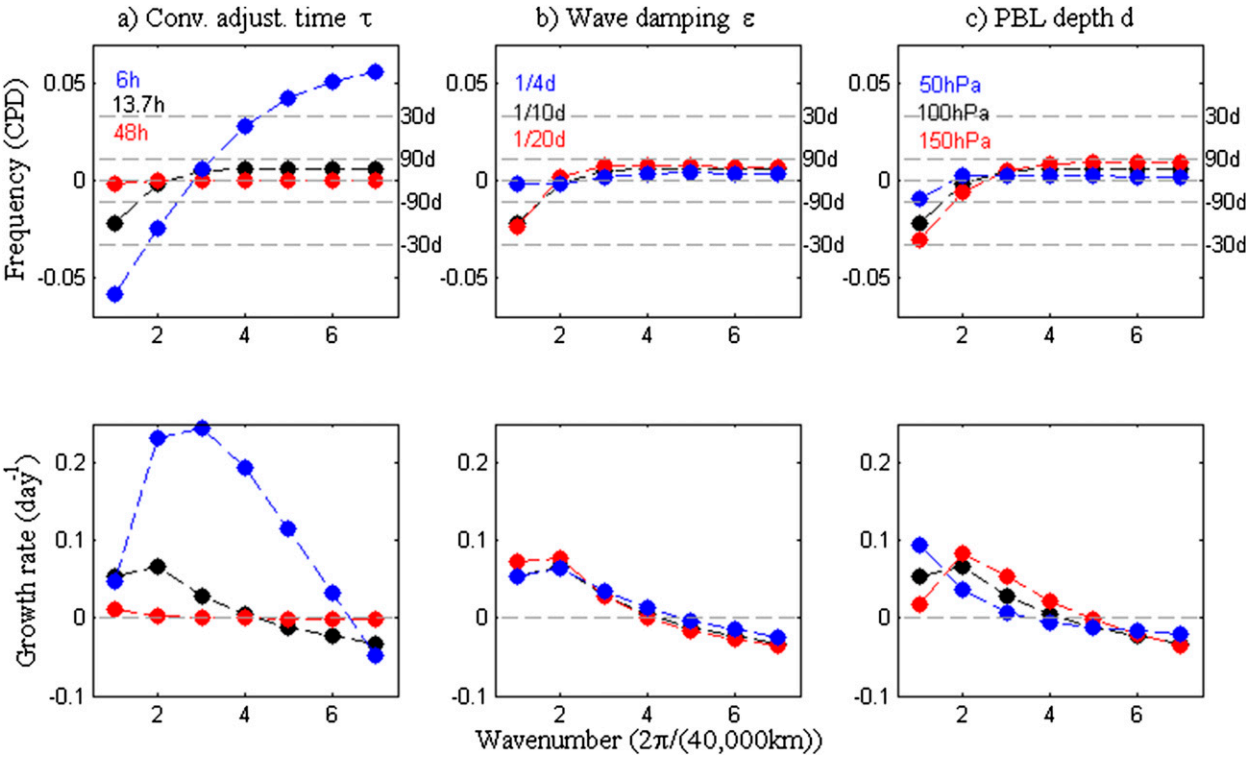

FIG. 13. As in Fig. 9, but showing the difference between the FCDM and FCM modes.

found to destabilize the MJO. The moisture feedback and wave feedback may have different effects on the simulated MJO modes when these processes are present. Among these different mechanisms, we only consider the simple frictional PBL process and focus on the roles of the moisture and wave feedbacks.

In this three-way interaction model, the slow convective adjustment process is preferred for simulating the MJO. Here, the slow adjustment process for the deep convection can be seen as a parameterization of the slow transition from shallow convection to deep convection. In this work, only the first baroclinic mode associated with the deep convection is included. The shallow convection, which plays a central role in the MJO propagation through moistening and preconditioning the atmosphere (Adames 2017), is not considered. Thus, the lower-tropospheric moisture anomaly associated with the shallow convection is assumed to be released slowly by deep convection through a slow convective adjustment process, while this parameterization needs further analysis using both theoretical models and general circulation models.

Acknowledgments. This work was supported by the China National 973 Project (2015CB453200), the National Natural Science Foundation of China (41420104002), grants from the IPOVAR Project (GASI-IPOVAI-02), and the Natural Science Foundation of Jiangsu Province (BK20150907). BW acknowledges supports from the NSF (Award AGS-1540783), the NOAA DYNAMO (Award NA13OAR4310167), and the National Research Foundation (NRF) of Korea through a Global Research Laboratory (GRL) grant (MEST, 2011-0021927). This paper is Earth System Modeling Center (ESMC) Contribution 184.

APPENDIX

Derivation of the Dispersion Relationship

Assuming that the solutions of the five variables have the structure of $\{u, \phi, q, p_r, w_b\} = \{U, \Phi, Q, P_r, W_b\}e^{i(kx-\sigma t)}$, Eq. (2) in the frequency–wavenumber space becomes

$$\begin{aligned} -i\sigma r_w U &= -ik\Phi - \varepsilon U, \\ -i\sigma r_w \Phi + ikU - W_b &= -P_r - \varepsilon\Phi, \\ -i\sigma r_q Q + ik\overline{Q}U - \overline{Q}_b W_b &= -P_r, \\ P_r &= \frac{1}{\tau}Q, \\ W_b &= -k^2 dd_1\Phi + ikdd_2\Phi - dd_1 U. \end{aligned} \tag{A1}$$

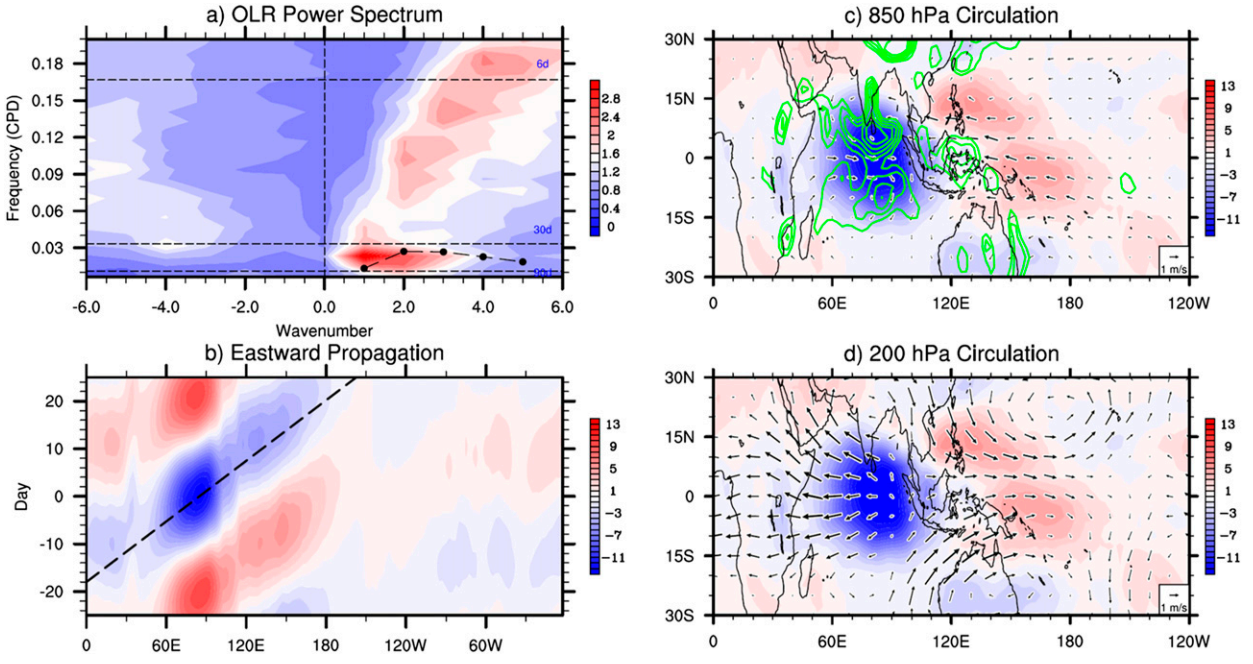

FIG. 14. Comparison with observations. (a) Wavenumber–frequency power spectrum of the symmetric component of OLR over 15°N–15°S from January 1979 to December 2013, plotted as the ratio between raw OLR power and the power in a smoothed red noise background spectrum (Wheeler and Kiladis 1999). The black dotted line shows the theoretical frequency in Fig. 2a. (b) Longitude–time evolution of intraseasonal (30–90-day bandpass filter) OLR anomalies (shading; W m^{-2}) over the tropics (10°N–10°S) by lag regression of OLR anomalies against itself averaged over the equatorial eastern Indian Ocean (10°N–10°S, 60°–100°E). The black dashed line denotes the theoretical phase speed of 6.2 m s^{-1}. (c) Regressed OLR (shading; W m^{-2}), 850-hPa horizontal winds (vectors; m s^{-1}), and upward vertical velocity at 850 hPa (contours; hPa s^{-1}) against OLR anomalies averaged over the equatorial eastern Indian Ocean. Vertical velocity contour interval is −0.2 hPa s^{-1}. (d) As in (c), but for 200-hPa horizontal winds.

When taking the zonal velocity U as a reference, other variables can be represented by using the first, second, fourth, and last equations in Eq. (A1).

$$\begin{aligned}
\Phi &= (i\varepsilon + \sigma r_w)k^{-1}U,\\
W_b &= [(-k^2 dd_1 + ikdd_2)(i\varepsilon + \sigma r_w)k^{-1} - dd_1]U,\\
P_r &= [(ir_w\sigma + idd_2k - dd_1k^2 - \varepsilon)(i\varepsilon + r_w\sigma)k^{-1} - ik - dd_1]U, \quad \text{and}\\
Q &= [(ir_w\sigma + idd_2k - dd_1k^2 - \varepsilon)(i\varepsilon + r_w\sigma)k^{-1} - ik - dd_1]\tau U. \qquad \text{(A2)}
\end{aligned}$$

The phase relationship between these variables can be calculated using Eq. (A2). After substituting Eq. (A2) into the moisture equation of Eq. (A1), we can obtain the dispersion relationship as follows:

$$\begin{aligned}
&r_q r_w^2 \tau\sigma^3 + [r_q(idd_1\tau k^2 + dd_2\tau k + 2i\varepsilon\tau) + ir_w]r_w\sigma^2\\
&\quad + [r_w dd_1(\overline{Q}_b - 1)k^2 - r_q\tau(\varepsilon dd_1 + 1)k^2 + ir_q d(\varepsilon d_2 + d_1)\tau k - ir_w dd_2(\overline{Q}_b - 1)k - r_q\varepsilon^2\tau - 2r_w\varepsilon]\sigma\\
&\quad + \varepsilon dd_1(\overline{Q}_b - 1)ik^2 + (\overline{Q} - 1)ik^2 + (\varepsilon d_2 + d_1)(\overline{Q}_b - 1)dk - i\varepsilon^2 = 0. \qquad \text{(A3)}
\end{aligned}$$

REFERENCES

Adames, Á. F., 2017: Precipitation budget of the Madden–Julian oscillation. *J. Atmos. Sci.*, **74**, 1799–1817, doi:10.1175/JAS-D-16-0242.1.

——, and D. Kim, 2016: The MJO as a dispersive, convectively coupled moisture wave: Theory and observations. *J. Atmos. Sci.*, **73**, 913–941, doi:10.1175/JAS-D-15-0170.1.

Betts, A. K., 1986: A new convective adjustment scheme. Part I: Observational and theoretical basis. *Quart. J. Roy. Meteor. Soc.*, **112**, 677–691, doi:10.1002/qj.49711247307.

——, and M. J. Miller, 1986: A new convective adjustment scheme. Part II: Single column tests using GATE wave, BOMEX, ATEX and Arctic air-mass data sets. *Quart. J. Roy. Meteor. Soc.*, **112**, 693–709, doi:10.1002/qj.49711247308.

Chen, G., and B. Wang, 2017: Reexamination of the wave activity envelope convective scheme in theoretical modeling of MJO. *J. Climate*, **30**, 1127–1138, doi:10.1175/JCLI-D-16-0325.1.

Chikira, M., 2014: Eastward-propagating intraseasonal oscillation represented by Chikira–Sugiyama cumulus parameterization. Part II: Understanding moisture variation under weak temperature gradient balance. *J. Atmos. Sci.*, **71**, 615–639, doi:10.1175/JAS-D-13-038.1.

Frierson, D. M. W., A. J. Majda, and O. M. Pauluis, 2004: Large scale dynamics of precipitation fronts in the tropical atmosphere: A novel relaxation limit. *Commun. Math. Sci.*, **2**, 591–626, doi:10.4310/CMS.2004.v2.n4.a3.

Fuchs, Ž., and D. J. Raymond, 2005: Large-scale modes in a rotating atmosphere with radiative convective instability and WISHE. *J. Atmos. Sci.*, **62**, 4084–4094, doi:10.1175/JAS3582.1.

——, and ——, 2017: A simple model of intraseasonal oscillations. *J. Adv. Model. Earth Syst.*, **9**, 1195–1211, doi:10.1002/2017MS000963.

Gill, A. E., 1980: Some simple solutions for heat-induced tropical circulation. *Quart. J. Roy. Meteor. Soc.*, **106**, 447–462, doi:10.1002/qj.49710644905.

Hendon, H. H., and B. Liebmann, 1994: Organization of convection within the Madden–Julian oscillation. *J. Geophys. Res.*, **99**, 8073–8083, doi:10.1029/94JD00045.

——, and M. L. Salby, 1994: The life cycle of the Madden–Julian oscillation. *J. Atmos. Sci.*, **51**, 2225–2237, doi:10.1175/1520-0469(1994)051<2225:TLCOTM>2.0.CO;2.

Hsu, P.-C., and T. Li, 2012: Role of the boundary layer moisture asymmetry in causing the eastward propagation of the Madden–Julian oscillation. *J. Climate*, **25**, 4914–4931, doi:10.1175/JCLI-D-11-00310.1.

Kalnay, E., and Coauthors, 1996: The NCEP/NCAR 40-Year Reanalysis Project. *Bull. Amer. Meteor. Soc.*, **77**, 437–471, doi:10.1175/1520-0477(1996)077<0437:TNYRP>2.0.CO;2.

Kang, I.-S., F. Liu, M.-S. Ahn, Y.-M. Yang, and B. Wang, 2013: The role of SST structure in convectively coupled Kelvin–Rossby waves and its implications for MJO formation. *J. Climate*, **26**, 5915–5930, doi:10.1175/JCLI-D-12-00303.1.

Kiladis, G. N., K. H. Straub, and P. T. Haertel, 2005: Zonal and vertical structure of the Madden–Julian oscillation. *J. Atmos. Sci.*, **62**, 2790–2809, doi:10.1175/JAS3520.1.

——, M. C. Wheeler, P. T. Haertel, K. H. Straub, and P. E. Roundy, 2009: Convectively coupled equatorial waves. *Rev. Geophys.*, **47**, RG2003, doi:10.1029/2008RG000266.

Kim, D., M.-S. Ahn, I.-S. Kang, and A. D. Del Genio, 2015: Role of longwave cloud–radiation feedback in the simulation of the Madden–Julian oscillation. *J. Climate*, **28**, 6979–6994, doi:10.1175/JCLI-D-14-00767.1.

Liebmann, B., and C. A. Smith, 1996: Description of a complete (interpolated) outgoing longwave radiation dataset. *Bull. Amer. Meteor. Soc.*, **77**, 1275–1277.

Liu, F., and B. Wang, 2012a: A frictional skeleton model for the Madden–Julian oscillation. *J. Atmos. Sci.*, **69**, 2749–2758, doi:10.1175/JAS-D-12-020.1.

——, and ——, 2012b: A model for the interaction between 2-day waves and moist Kelvin waves. *J. Atmos. Sci.*, **69**, 611–625, doi:10.1175/JAS-D-11-0116.1.

——, and ——, 2013a: An air–sea coupled skeleton model for the Madden–Julian oscillation. *J. Atmos. Sci.*, **70**, 3147–3156, doi:10.1175/JAS-D-12-0348.1.

——, and ——, 2013b: Impacts of upscale heat and momentum transfer by moist Kelvin waves on the Madden–Julian oscillation: A theoretical model study. *Climate Dyn.*, **40**, 213–224, doi:10.1007/s00382-011-1281-0.

——, and ——, 2016: Role of horizontal advection of seasonal-mean moisture in the Madden–Julian oscillation: A theoretical model analysis. *J. Climate*, **29**, 6277–6293, doi:10.1175/JCLI-D-16-0078.1.

——, and ——, 2017: Effects of moisture feedback in a frictional coupled Kelvin–Rossby wave model and implication in the Madden–Julian oscillation dynamics. *Climate Dyn.*, **48**, 513–522, doi:10.1007/s00382-016-3090-y.

——, G. Huang, and L. Feng, 2012: Critical roles of convective momentum transfer in sustaining the multi-scale Madden–Julian oscillation. *Theor. Appl. Climatol.*, **108**, 471–477, doi:10.1007/s00704-011-0541-6.

Majda, A. J., and J. A. Biello, 2004: A multiscale model for tropical intraseasonal oscillations. *Proc. Natl. Acad. Sci. USA*, **101**, 4736–4741, doi:10.1073/pnas.0401034101.

——, and S. N. Stechmann, 2009: The skeleton of tropical intraseasonal oscillations. *Proc. Natl. Acad. Sci. USA*, **106**, 8417–8422, doi:10.1073/pnas.0903367106.

——, ——, and B. Khouider, 2007: Madden–Julian oscillation analog and intraseasonal variability in a multicloud model above the equator. *Proc. Natl. Acad. Sci. USA*, **104**, 9919–9924, doi:10.1073/pnas.0703572104.

Maloney, E. D., and D. L. Hartmann, 1998: Frictional moisture convergence in a composite life cycle of the Madden–Julian oscillation. *J. Climate*, **11**, 2387–2403, doi:10.1175/1520-0442(1998)011<2387:FMCIAC>2.0.CO;2.

Matsuno, T., 1966: Quasi-geostrophic motions in the equatorial area. *J. Meteor. Soc. Japan*, **44**, 25–43, doi:10.2151/jmsj1965.44.1_25.

Nakazawa, T., 1988: Tropical super clusters within intraseasonal variations over the western Pacific. *J. Meteor. Soc. Japan*, **66**, 823–839, doi:10.2151/jmsj1965.66.6_823.

Raymond, D. J., and Ž. Fuchs, 2007: Convectively coupled gravity and moisture modes in a simple atmospheric model. *Tellus*, **59A**, 627–640, doi:10.1111/j.1600-0870.2007.00268.x.

Rui, H., and B. Wang, 1990: Development characteristics and dynamic structure of tropical intraseasonal convection anomalies. *J. Atmos. Sci.*, **47**, 357–379, doi:10.1175/1520-0469(1990)047<0357:DCADSO>2.0.CO;2.

Sobel, A., and E. Maloney, 2012: An idealized semi-empirical framework for modeling the Madden–Julian oscillation. *J. Atmos. Sci.*, **69**, 1691–1705, doi:10.1175/JAS-D-11-0118.1.

——, and ——, 2013: Moisture modes and the eastward propagation of the MJO. *J. Atmos. Sci.*, **70**, 187–192, doi:10.1175/JAS-D-12-0189.1.

Sperber, K. R., 2003: Propagation and the vertical structure of the Madden–Julian oscillation. *Mon. Wea. Rev.*, **131**, 3018–3037, doi:10.1175/1520-0493(2003)131<3018:PATVSO>2.0.CO;2.

Tian, B., D. E. Waliser, E. J. Fetzer, B. H. Lambrigtsen, Y. L. Yung, and B. Wang, 2006: Vertical moist thermodynamic structure and spatial–temporal evolution of the MJO in AIRS observations. *J. Atmos. Sci.*, **63**, 2462–2485, doi:10.1175/JAS3782.1.

Wang, B., 1988: Dynamics of tropical low-frequency waves: An analysis of the moist Kelvin wave. *J. Atmos. Sci.*, **45**, 2051–2065, doi:10.1175/1520-0469(1988)045<2051:DOTLFW>2.0.CO;2.

——, and H. Rui, 1990: Dynamics of the coupled moist Kelvin–Rossby wave on an equatorial β-plane. *J. Atmos. Sci.*, **47**, 397–413, doi:10.1175/1520-0469(1990)047<0397:DOTCMK>2.0.CO;2.

——, and X. Xie, 1998: Coupled odes of the warm pool climate system. Part I: The role of air–sea interaction in maintaining Madden–Julian oscillation. *J. Climate*, **11**, 2116–2135, doi:10.1175/1520-0442-11.8.2116.

——, and F. Liu, 2011: A model for scale interaction in the Madden–Julian oscillation. *J. Atmos. Sci.*, **68**, 2524–2536, doi:10.1175/2011JAS3660.1.

——, and G. Chen, 2017: A general theoretical framework for understanding essential dynamics of Madden–Julian oscillation. *Climate Dyn.*, **49**, 2309–2328, doi:10.1007/s00382-016-3448-1.

——, F. Liu, and G. Chen, 2016: A trio-interaction theory for Madden–Julian oscillation. *Geosci. Lett.*, **3**, 34, doi:10.1186/s40562-016-0066-z.

Wang, L., T. Li, E. Maloney, and B. Wang, 2017: Fundamental causes of propagating and nonpropagating MJOs in MJOTF/GASS models. *J. Climate*, **30**, 3743–3769, doi:10.1175/JCLI-D-16-0765.1.

Wheeler, M., and G. N. Kiladis, 1999: Convectively coupled equatorial waves: Analysis of clouds and temperature in the wavenumber–frequency domain. *J. Atmos. Sci.*, **56**, 374–399, doi:10.1175/1520-0469(1999)056<0374:CCEWAO>2.0.CO;2.

Yang, D., and A. P. Ingersoll, 2013: Triggered convection, gravity waves, and the MJO: A shallow-water model. *J. Atmos. Sci.*, **70**, 2476–2486, doi:10.1175/JAS-D-12-0255.1.

——, and ——, 2014: A theory of the MJO horizontal scale. *Geophys. Res. Lett.*, **41**, 1059–1064, doi:10.1002/2013GL058542.

Zhang, C., 2005: Madden–Julian Oscillation. *Rev. Geophys.*, **43**, RG2003, doi:10.1029/2004RG000158.